

Synthesis, characterization, and application of nickel oxide/CNT nanocomposites to remove Pb^{2+} from aqueous solution

T. Navaei Diva¹ · K. Zare¹  · F. Taleshi² · M. Yousefi¹

Received: 9 June 2017 / Accepted: 26 July 2017 / Published online: 31 July 2017
© The Author(s) 2017. This article is an open access publication

Abstract In this study, the efficiency of nickel oxide/carbon nanotube (NiO/CNT) nanocomposite to remove Pb^{2+} from aqueous solution is investigated. NiO/CNT nanocomposite was prepared using the direct coprecipitation method in an aqueous media in the presence of CNTs. Samples were characterized using simultaneous thermal analysis (STA), X-ray diffraction (XRD), field emission scanning electron microscopy (FESEM), and Brunauer–Emmett–Teller (BET). To optimize the adsorption of Pb^{2+} ions on NiO/CNT nanocomposite, the effects of different parameters including pH, contact time, initial concentration of Pb^{2+} , and adsorbent mass—were also investigated. The optimum Pb^{2+} removal efficiency on NiO/CNT nanocomposite is achieved under experimental conditions of pH 7, contact time of 10 min, initial Pb^{2+} concentration of 20 ppm, and adsorbent mass of 0.1 g. The experimental data showed that the Pb^{2+} ions adsorption of NiO/CNT nanocomposite was through a Freundlich isotherm model rather than a Langmuir model. The kinetic data of adsorption of Pb^{2+} ions on the adsorbent was perfectly shown by a pseudo-second-order equation, to indicate their chemical adsorption. Thermodynamic parameters such as ΔG° , ΔH° , and ΔS° were also measured; the obtained values showed that the adsorption was basically spontaneous and endothermic.

Keywords Removal · Adsorption · Carbon nanotubes · Composite · Heavy metals

Introduction

Water, which is one of the main elements in the environment, is highly exposed to contamination. Among water pollutants, heavy metal cations, including Pb^{2+} , Cd^{2+} , Cr^{3+} , Cr^{6+} , Co^{2+} , Cu^{2+} , Fe^{3+} , Ni^{2+} and Zn^{2+} , are extremely toxic and non-biodegradable. These are commonly discharged into water sources and environment via either natural or industrial wastes. Today, elimination of water sources from such cations is among the main challenges faced by researchers and environmentalists. The accumulation of these metal cations in living organisms causes many physiological disorders [1]. The permitted level of Pb^{2+} in drinking water is 0.01 mg L^{-1} [2]. The exposure of human body organs to high concentrations of Pb^{2+} can result in anaemia, mental disorder, and renal and liver diseases.

Several different methods have been introduced and used for heavy metal removal [3], i.e. chemical precipitation, ion exchange, reverse osmosis, membrane-based processes, evaporation, solvent extraction, and adsorption. The efficiency of some of these methods is reduced due to major drawbacks including low removal efficiency and causing side effects that lead to new environmental issues.

In recent years, metal oxide nanoparticles especially metal oxide/CNT nanocomposites have attracted a good deal of persistent interest because of their unique chemical, physical, electrical, and thermal properties [4–6]. These materials are widely used in several areas, including chemistry, physics, material science, biology, medicine, and environment [7, 8].

✉ K. Zare
k-zare@sbu.ac.ir

¹ Department of Chemistry, Science and Research Branch, Islamic Azad University, Tehran, Iran

² Department of Physics, Qaemshahr Branch, Islamic Azad University, Qaemshahr, Iran

Metal oxide nanoparticle and metal oxide/CNT nanocomposite adsorbents have been applied for the removal of heavy metals from aqueous solutions. These adsorbents are economically more affordable and also more environment-friendly [9–12].

The amount of heavy metal uptake is directly associated with the total amount of active sites available on the adsorbent; a decrease in metallic nanoparticle dimensions increases their surface-to-volume ratio and consequently increases the active surface area for adsorption. In this regard, the utilization of appropriate substrate material in the synthesis procedure of metal oxide nanoparticles can prevent agglomeration, decrease the diameter of nanoparticles, and change the cluster-like morphology of nanoparticles to a powdered morphology. Therefore, the obtained nanocomposite with larger specific surface area and higher adsorption capacity can be employed as a suitable adsorbent for heavy metal removal.

Due to high surface-to-volume ratio, CNTs are considered as great substrates for the nucleation and growth of nanoparticles with control over diameter distribution [13–16]. One of the main challenges encountered when CNTs are used as the support material for nanoparticle synthesis is the hydrophobicity of their surface. In this regard, surface functionalization of CNTs for the generation of covalent bonds and further attachment of oxide nanoparticles seems to be of great significance [17–19]. The functionalization of CNTs is commonly performed using the chemical oxidation process introducing functional groups such as $-\text{COOH}$, $\text{C}-\text{O}$, $\text{C}=\text{O}$, and $-\text{OH}$ on the surface of CNTs; such groups act as active surface sites for metal attachment [20, 21]. NiO nanostructure can be synthesized through various methods such as co-precipitation [22], sol gel [23], hydrothermal [24], spray pyrolysis method [25], and chemical precipitation [26]. In this study, NiO/CNT nanocomposite was synthesized by chemical precipitation method, which was simple and cost efficient.

NiO/CNT nanocomposite was applied as an adsorbent to remove Pb^{2+} from aqueous solution. However, pH, contact time, adsorbent dosage, and initial concentration of Pb^{2+} were the parameters, the effects of which on adsorption uptake have been investigated.

Experiment

Materials

Lead nitrate [$\text{Pb}(\text{NO}_3)_2$, 99.5%], nickel chloride hexahydrate ($\text{NiCl}_2 \cdot 6\text{H}_2\text{O}$, 98%), sodium hydroxide (NaOH, 99%), CNTs (MWCNTs, US4309, $20 < d < 30$ nm,

$\text{SSA} = 264 \text{ m}^2 \text{ g}^{-1}$, 95%), and sulphuric (95–97%), nitric (60%), and hydrochloric (37%) acids were applied without further purification.

To synthesize NiO/CNT nanocomposite, the surface of CNTs was functionalized as follows: initially, the desired amount of CNTs was added to the mixture of sulphuric/nitric/hydrochloric acids (6 M) and ultrasonicated for 30 min. The obtained mixture was stirred for 2 h at temperature of 80°C and was then filtered and washed with deionized water until the pH reached 7. Finally, the functionalized CNTs were dried in an oven at 120°C .

For NiO/CNT nanocomposite preparation with 1:1 weight ratio, 3.2 g of $\text{NiCl}_2 \cdot 6\text{H}_2\text{O}$ was dissolved in 50 ml of deionized water containing 1 g of functionalized CNTs. This was then ultrasonicated for 10 min and magnetically stirred for 15 min at 80°C . The addition of 1.1 g of NaOH to the mixture and stirring for 30 min completed the precipitation of $\text{Ni}(\text{OH})_2/\text{CNTs}$ nanocomposite. The obtained black mixture was filtered, washed with absolute ethanol and deionized water, dried at 120°C for 24 h, and finally calcinated at 300°C for 2 h in static air.

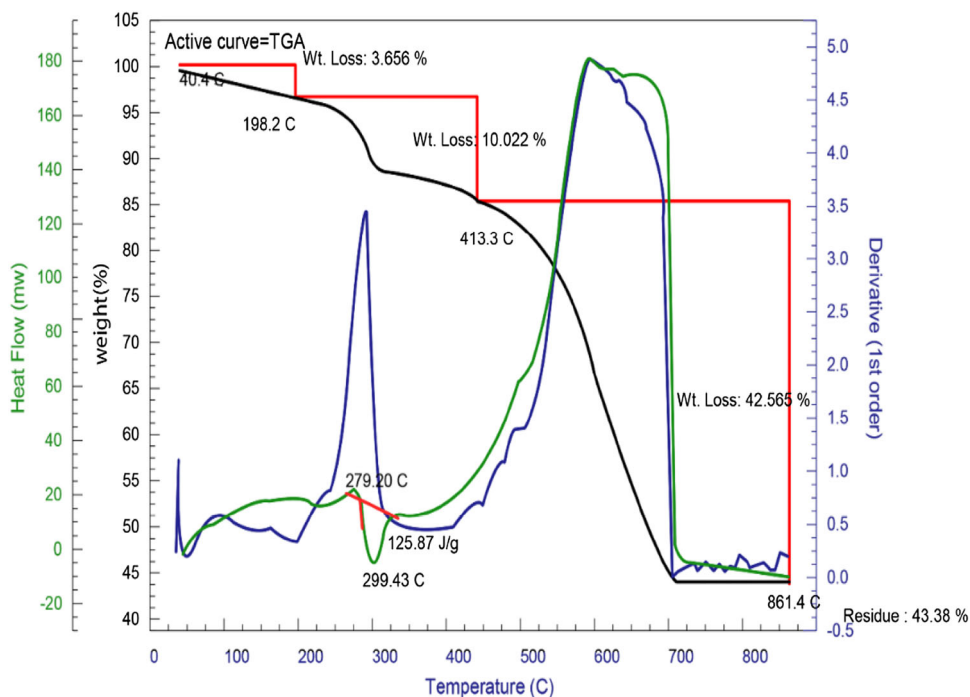
Methods of analysis

To determine the optimum calcination temperature of NiO/CNT nanocomposite powder, simultaneous thermal analysis (STA 1500) was applied in a static air atmospheric ($10^\circ\text{C min}^{-1}$). The residual concentration of Pb^{2+} ions in aqueous media was analysed with the aid of Buck Scientifics 210 VGP flame atomic adsorption spectroscopy. The crystallinity of samples was determined using Xpertpr Pananalytical X-ray diffraction apparatus (Holland) with $\text{Cu}(\text{K}_\alpha)$ source and wavelength of $\lambda = 1.5405 \text{ \AA}$. The morphology of powders was recorded using Field Emission Scanning Electron Microscopy on a Mira3-XMU system. The BET specific surface area and porosity were determined using nitrogen adsorption-desorption porosimetry (77 K) by a porosimeter (Bel Japan, Inc.).

Adsorption studies

In this section, 1000 ppm of Pb^{2+} stock solution was initially provided through dissolving the desired volume of ($\text{Pb}(\text{NO}_3)_2$) in deionized water; the corresponding concentrations were then obtained from the dilution of the stock solution. For batch adsorption experiments, 0.1 g of NiO/CNT was added to 50 ml of 20 ppm solution of Pb^{2+} and then stirred. After adsorption, the nanocomposite was



Fig. 1 STA curves of Ni(OH)₂/CNT in air

taken from the solution and the residual Pb²⁺ concentration was measured using flame atomic adsorption spectroscopy. The effects of the different parameters namely pH, initial Pb²⁺ concentration, adsorbent dosage, and contact time on the amount of adsorption were investigated through the removal percentage (*R*) of Pb²⁺ by the equation mentioned below:

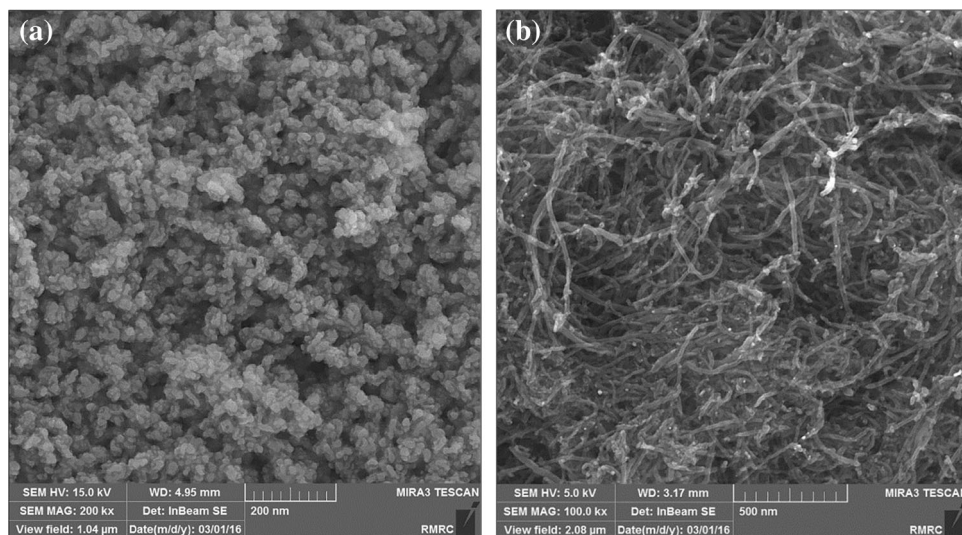
$$\%R = \frac{C_0 - C_e}{C_0} \times 100,$$

here, *C*₀ and *C*_{*e*} are the initial and equilibrium concentrations of Pb²⁺ (mg L⁻¹).

Result and discussion

NiO/CNT characterization

To study the temperature-dependent behaviour of nanocomposite, STA was performed on Ni(OH)₂/CNT synthesized precursor in static air. According to the obtained spectra (Fig. 1), in the temperature range of 40–800 °C, three endothermic reactions occur in Ni(OH)₂/CNT. In the range of 40–400 °C, two stages of weight loss in the sample are observed. These can be attributed to two reactions in the initial stage at 40–200 °C, attributing to

Fig. 2 FESEM of **a** pure NiO and **b** NiO/CNT nanocomposite

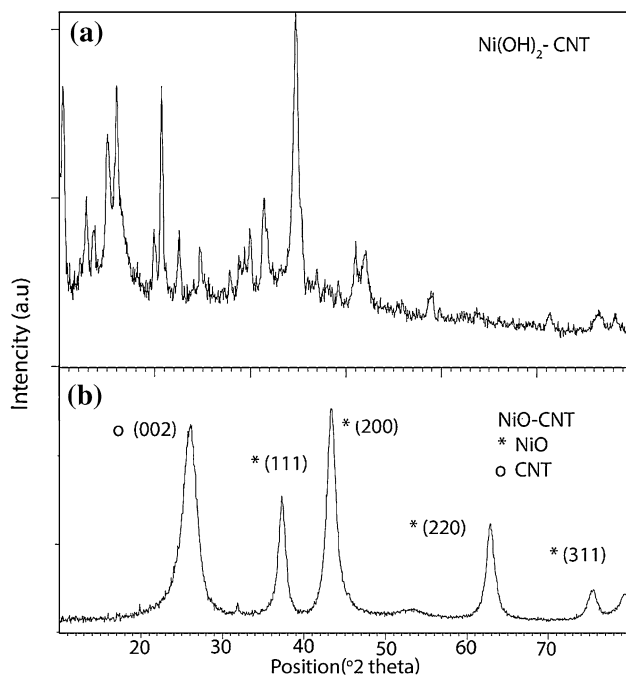


Fig. 3 XRD pattern of **a** Ni(OH)₂/CNT and **b** NiO/CNT nanocomposite

surface moisture evaporation and the second one at 200–400 °C is the result of water release and the formation of NiO chemical structure with the following reactions:

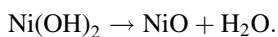
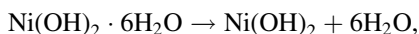


Fig. 5 **a** Effect of pH, **b** contact time, **c** adsorbent mass and **d** initial concentration on Pb²⁺ removal by NiO/CNT nanocomposite

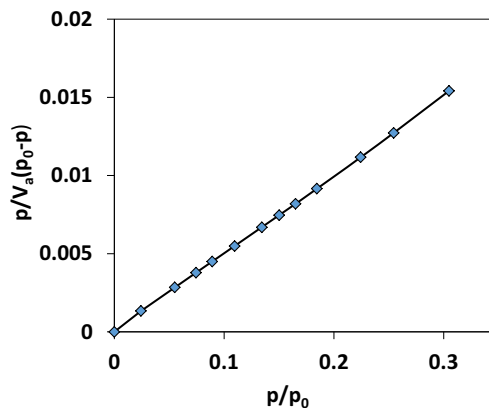
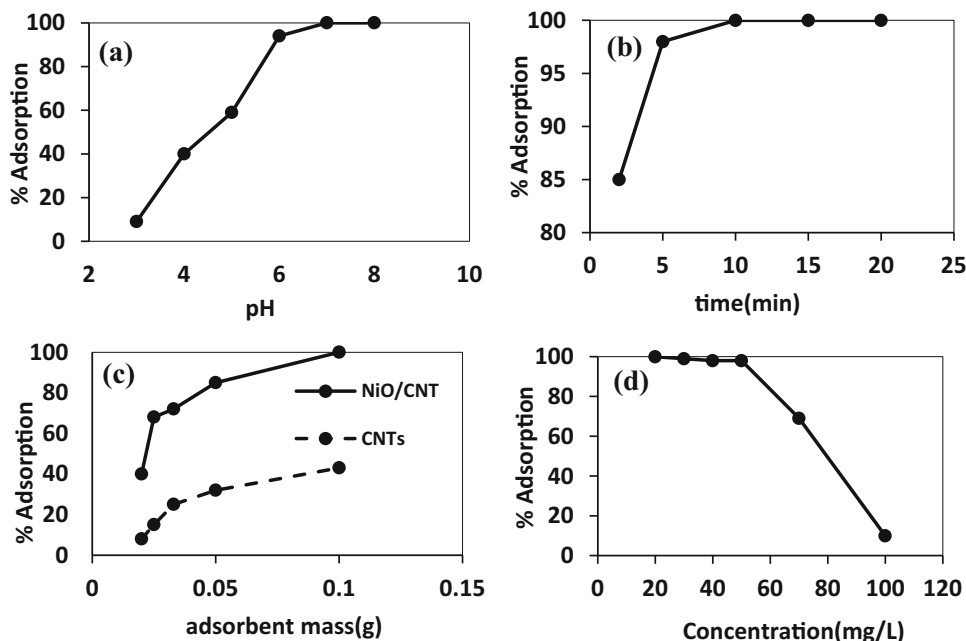


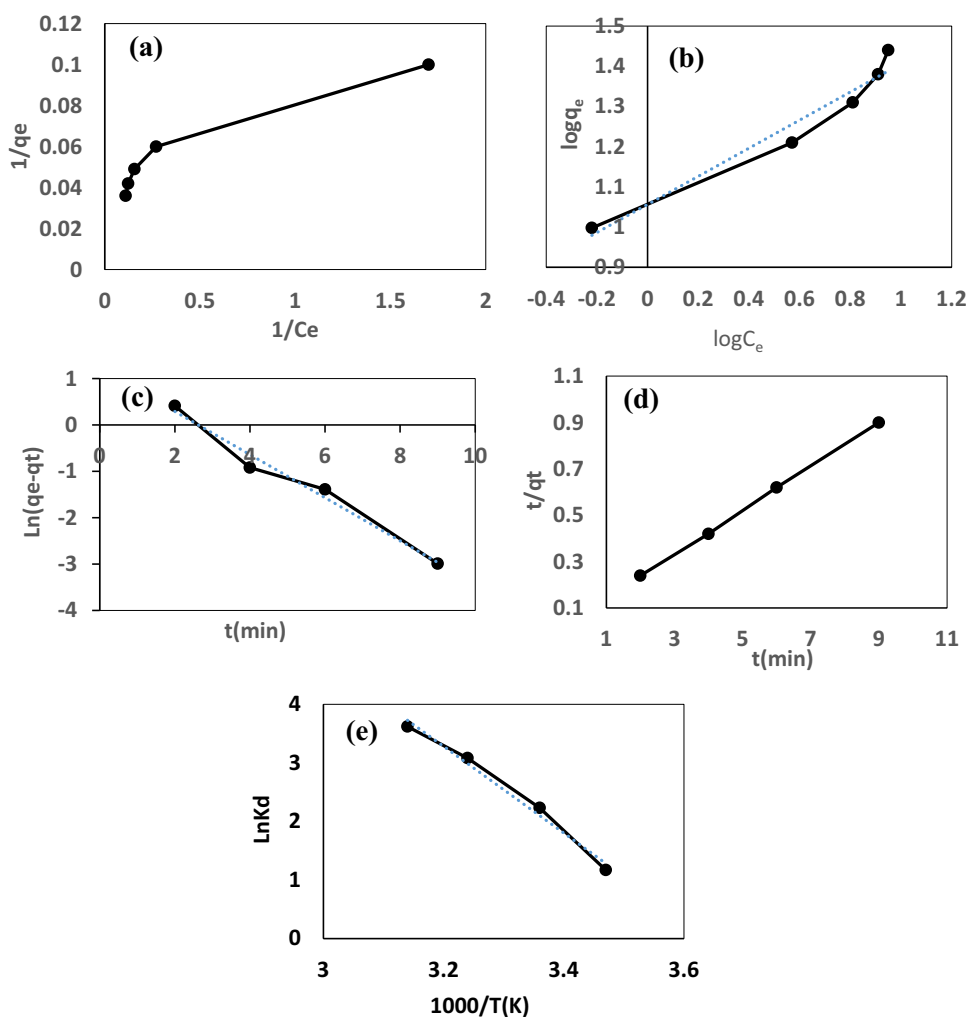
Fig. 4 BET plot of NiO/CNT nanocomposite

The slow decrease in weight at a temperature above 300 °C is related to the removal of small amounts of hydroxyl-groups remaining during the development of the NiO phase [27].

The weight percentage of the sample at 400 °C was 86%, which is related to the NiO/CNT nanocomposite. At 800 °C, the weight percentage of the sample reached 43%, due to the oxidation of CNTs into CO₂ [28]. Following the specifications of STA, 300 °C was considered as the reaction temperature in the study.

The morphologies of NiO/CNT and pure NiO were analysed using FESEM images, as shown in Fig. 2. It can be seen in Fig. 2a that NiO nano-crystallites are aggregated, forming clusters with larger grains. The formation of this agglomerated structure has unfavourable impacts on

Fig. 6 **a** Langmuir, **b** Freundlich adsorption isotherm, **c** pseudo-first-order, **d** pseudo-second-order kinetic models and **e** Van't Hoff plot for Pb^{2+} removal on NiO/CNT nanocomposite



the physical and chemical features of nanoparticles. The utilization of CNTs as the support material for the growth of nanoparticles reduces the agglomeration and changes the powder morphology from a cluster-like to a filamentous structure (Fig. 2b). It is observed that the nanoparticles on the surface of CNTs possess smaller dimensions in comparison with pure NiO nanoparticles [27].

Figure 3 indicates the X-ray diffraction pattern of $\text{Ni}(\text{OH})_2/\text{CNT}$ and NiO/CNT nanocomposites. Characteristic peaks at $2\theta = 37.3^\circ$, 43.4° , 62.9° and 75.4° are assigned to (111), (200), (220), and (311) crystallographic orientations in NiO nanoparticles, respectively (Fig. 3a), the strong diffraction peak at $2\theta = 26^\circ$ reflected from (002) lattice plane in CNTs [29]. The peaks of $\text{Ni}(\text{OH})_2/\text{CNT}$ cannot be seen at NiO/CNT, which is due to the crystallization and change in the structure of crystal. The size of NiO/CNT nanoparticles was calculated using the Scherrer equation $D = \frac{k\lambda}{\beta \cos \theta}$. The main reflection peak of the XRD pattern at $2\theta = 43^\circ$ can be attributed to (200) plane. The size of NiO/CNT nano-crystallites was 18.5 nm.

N_2 adsorption–desorption isotherms was utilized to assess the specific surface area, mean pore diameter and the total volume of NiO/CNT nanocomposite. The specific surface area of NiO/CNT nanocomposite was measured by the Brunauer–Emmett–Teller (BET) method (Fig. 4). The specific surface area, mean pore diameter and the total pore volume of NiO/CNT nanocomposite were determined to be $90 \text{ m}^2 \text{ g}^{-1}$, 4.16 nm and $9.26 \times 10^{-2} \text{ cm}^3 \text{ g}^{-1}$, respectively.

Effect of pH

The pH is among the most remarkable parameters that should be controlled in metal ions adsorption process of aqueous solutions. To evaluate the effect of pH, the initial pH varied from 3 to 8 in the solution. It was observed (Fig. 5a) that the rate of removal of Pb^{2+} increased rapidly, from about 9–94% as pH increased from 3 to 6, and then remained constant following the increase of pH value from 7 to 8. Based on the authors' best knowledge, lead species are available in Pb^{2+} and $\text{Pb}(\text{OH})^+$ forms at pH 3–8 [30].

Table 1 Langmuir, Freundlich parameters and correlation coefficients of Pb²⁺ adsorption onto NiO/CNT

Langmuir	$\frac{1}{q_e} = \left(\frac{1}{q_m K_L}\right) + \left(\frac{1}{C_e}\right) + \frac{1}{q_m}$		Freundlich	$\log q_e = \log K_F + \frac{1}{n} \log C_e$	
q_m (mg g ⁻¹)	K_L (L mg ⁻¹)	R^2	K_F (L mg ⁻¹)	$1/n$	R^2
24.63	1.14	0.9279	11.39	0.3493	0.9502

Table 2 The equilibrium capacities of Pb(II) on various adsorbents

Adsorbents	q_{max} (mg g ⁻¹)	References
MWCNTs	1	[35]
MWCNTs	4	[36]
Activated carbon	13.05	[37]
MWCNTs	15.6	[35]
Oxidized MWCNTs	2.06	[38]
Oxidized N-doped MWCNTs	29	[39]
MWCNT-f	14.56	[40]
TiO ₂ /CNT	65.52	[41]
SiO ₂ /MWCNT	13	[42]
Iron oxid/MWCNT	12	[43]
Al ₂ O ₃ /CNTs	67.5	[44]
PAAM/MWCNTs	29.71	[45]
Zeolites: chabazite	6	[46]
NiO/CNTs	24.63	This study

When the pH value is low (<6), the predominant lead specie is Pb²⁺ and Pb²⁺ is removed by sorption reaction. Therefore, the lower adsorption percentage of Pb²⁺ on NiO/CNT at lower pH values partly depends on the competition between H⁺ and Pb²⁺ on the surface sites Pb²⁺ removal rate, which is maximized in pH values 6 to 8 and then remains constant. In this range, the main species are Pb²⁺ and Pb(OH)⁺; hence, Pb²⁺ removal is regulated by the sorption of Pb²⁺ and Pb(OH)⁺. According to the results of the current study, to eliminate Pb²⁺ from the solution by NiO/CNT, pH 7 is the most optimum value for the employed system.

Effect of contact time

The contact time and its effect on Pb²⁺ elimination rate using NiO/CNT is depicted in Fig. 5b. The highest amount of adsorption approximately 100%, was achieved after 10 min of adsorption at pH 7. Therefore, a period of 10 min was considered as the optimum contact time for Pb²⁺ adsorption on the NiO/CNT nanocomposite.

Effect of adsorbent mass

Figure 5c illustrates the effect of adsorbent mass on the removal rate for a 20 ppm solution of Pb²⁺ by NiO/CNT

nanocomposite and CNTs. In both adsorbents, the percentage of adsorbed lead increased as the mass of adsorbent was increased over the range of 0.02–0.1 g. A removal rate of approximately 100% was obtained when 0.1 g of NiO/CNT nanocomposite was drowned in 50 mL of the 20 ppm Pb²⁺ solution, compared to 43% removal when 0.1 g of CNTs was used. Based on the given results, it is obvious that the mechanism of nanocomposite adsorption towards Pb²⁺ may be attributed to three factors: the van der Waals interaction between the hexagonally arrayed carbon atoms in the graphite sheets of the CNTs and the positively charged lead ions, the electrostatic attraction between the negatively charged adsorbent surface of the CNT and Pb²⁺ cations, and the electrostatic attraction between Pb²⁺ and the electron pairs on the oxygen atoms of nickel oxide [30].

Effect of Pb²⁺ initial concentration

Figure 5d indicates the variation in removal rate in the initial concentration of Pb²⁺. It is evident that the initial concentration increase of Pb²⁺ from 20 to 100 ppm reduces the removal efficiency from almost 100–10%. At lower initial concentrations of Pb²⁺, an adequate number of active sites are available for adsorption, leading to a higher adsorption capacity. It is also noteworthy that at higher initial concentrations, the number of metal ions is higher compared with active adsorption sites; therefore, the removal efficiency decreases [31].

Adsorption isotherms

Adsorption isotherms represent the amount of adsorbed metal ion per unit mass of the adsorbent. Among all the isotherm models, the Langmuir and Freundlich models are the most popular ones describing adsorption in these systems [32–34]. The equilibrium adsorption capacity (q_e) is calculated using:

$$q_e = \frac{C_0 - C_e}{m} V,$$

here q_e is the adsorbed Pb²⁺ amount (mg g⁻¹), m is the composite mass (g), and V is the solution volume (L).

Figure 6a, b, respectively, illustrate Langmuir and Freundlich isotherms for Pb²⁺ adsorption on NiO/CNT nanocomposite with the obtained parameters summarized in Table 1. According to the data shown in Table 1, both the Langmuir and Freundlich models are appropriate for

Table 3 Adsorption kinetic parameters of Pb^{2+} adsorption onto NiO/CNT

Pseudo-first-order $\ln(q_e - q_t) = \ln q_e - k_1 t$			Pseudo-second-order $\frac{t}{q_t} = \frac{1}{k_2 q_e^2} + \frac{1}{q_e} t$			Experimental data
k_1 (min^{-1})	$q_{e,\text{cal}}$ ($\text{g mg}^{-1} \text{min}^{-1}$)	R^2	k_2 ($\text{g mg}^{-1} \text{min}^{-1}$)	$q_{e,\text{cal}}$ (mg g^{-1})	R^2	$q_{e,\text{exp}}$ (mg g^{-1})
0.46	16.54	0.9787	0.189	10.55	0.9997	10

Table 4 Values of thermodynamic parameters of adsorption of Pb^{2+} onto NiO/CNT

$\ln K_d = \frac{\Delta S^\circ}{R} - \frac{\Delta H^\circ}{RT}$		ΔG° (temperature, K)			
ΔS°	ΔH°	$\Delta G^\circ = -RT \ln K_d$		$K_d = \frac{q_e}{C_e}$	
224.26	61.55	2.80 (288)	-5.52 (298)	-7.89 (308)	-9.57 (318)

interpreting the obtained experimental data; however, the Freundlich model, with a higher correlation coefficient (R^2), showed higher compatibility with the data, compared with the Langmuir model.

To get the synthesized adsorbent efficiency approved, its maximum amount of adsorption was compared with other adsorbents. As shown in Table 2, the maximum adsorption capacity obtained in this study is significant compared to other adsorbents [35–46], which indicates the efficiency of the synthetic adsorbent.

Adsorption kinetics

One of the most important features of designing an adsorption system is the prediction of the adsorption rate, i.e., how fast the adsorption is taking place, which is controlled by adsorption kinetics. The adsorption kinetics depends on the adsorbent physical and chemical properties; it also affects the adsorption mechanism. To evaluate the adsorption mechanism, adsorption kinetic constants, Lagergren pseudo first-order and Ho, pseudo second-order rate equations can be used [47].

The obtained results are summarized in Fig. 6c, d, and Table 3. According to Table 3, the pseudo second-order model, with higher values of correlation coefficient (R^2) and closer values of calculated adsorption capacity ($q_{e,\text{cal}}$) to experimental one ($q_{e,\text{exp}}$) is a better model to describe the adsorption capacity of ions on NiO/CNT nanocomposite. This indicates that the adsorption of Pb^{2+} onto NiO/CNT may be the chemisorption involving valence forces through the exchange or sharing of electrons between adsorbate and adsorbent [48].

Adsorption thermodynamics

Another feature of any adsorption process with high significance is the determination of thermodynamic parameters, including changes in Gibbs free energy (ΔG° , KJ mol^{-1}), enthalpy (ΔH° , KJ mol^{-1}), and entropy (ΔS° ,

$\text{J mol}^{-1} \text{K}^{-1}$). Adsorption thermodynamics were evaluated at different temperatures (288, 298, 308, and 318 K). The results are depicted in Fig. 6e. To measure the thermodynamic parameters and K_d values, Van't Hoff equation was applied [49].

The results of calculation are shown in Table 4. The negative values of ΔG° indicate that the adsorption was a spontaneous reaction. The ΔH° and ΔS° positive values are attributed to the endothermic nature of adsorption and the increase in the randomness at the solid/liquid interface during the adsorption of Pb^{2+} on NiO/CNT nanocomposite, respectively.

Conclusion

In this study, NiO/CNT nanocomposite was utilized as an adsorbent to remove Pb^{2+} from an aqueous solution. The NiO/CNT nanocomposite powder was prepared using direct coprecipitation process in the aqueous media. The results indicate that the optimum efficiency for Pb^{2+} removal is achieved under experimental conditions of pH 7, contact time of 10 min, and the initial Pb^{2+} concentration of 20 ppm. Moreover, increasing the initial concentration of Pb^{2+} and reducing the adsorbent dosage diminishes the removal efficiency. Therefore, NiO/CNT nanocomposite can be considered as a useful adsorbent for the elimination of aqueous solutions from Pb^{2+} . In addition, results obtained from Pb^{2+} adsorption on NiO/CNT nanocomposite follow the pseudo second-order rate equation and Freundlich isotherm.

Open Access This article is distributed under the terms of the Creative Commons Attribution 4.0 International License (<http://creativecommons.org/licenses/by/4.0/>), which permits unrestricted use, distribution, and reproduction in any medium, provided you give appropriate credit to the original author(s) and the source, provide a link to the Creative Commons license, and indicate if changes were made.



References

1. Bedelean, H., Maicaneanu, A., Burca, S., Stanca, M.: Removal of heavy metal ions from wastewaters using natural clays. *J. Clay Miner.* **44**, 487–495 (2009)
2. Chand, P., Pakade, Y.B.: Synthesis and characterization of hydroxyapatite nanoparticles impregnated on apple pomace to enhanced adsorption of Pb(II), Cd(II) and Ni(II) ions from aqueous solution. *Environ. Sci. Pollut. Res.* **22**, 10919–10929 (2015)
3. Shafaei, A., Ashtiani, F.Z., Kaghazchi, T.: Equilibrium studies of the sorption of Hg(II) ions onto chitosan. *Chem. Eng. J.* **133**(1–3), 311–316 (2007)
4. Kumar, R., Singh, R.K., Dubey, P.K., Singh, D.P., Yadav, R.M., Tiwari, R.S.: Freestanding 3D graphene–nickel encapsulated nitrogen-rich aligned bamboo like carbon nanotubes for high-performance supercapacitors with robust cycle stability. *Adv. Mater. Interfaces* **2**, 1500191 (2015)
5. Kumar, R., Singh, R.K., Singh, D.P., Vaz, A.R., Yadav, R.R., Rout, C.S., Moshkalev, S.A.: Synthesis of self-assembled and hierarchical palladium-CNTs-reduced graphene oxide composites for enhanced field emission properties. *Mater. Des.* **122**, 110–117 (2017)
6. Kumar, R., Singh, R.K., Dubey, P.K., Singh, D.P., Yadav, R.M.: Self-assembled Hierarchical formation of conjugated 3D cobalt oxide nanobeads–CNTs–graphene nanostructure using microwave for high performance supercapacitor electrode. *ACS Appl. Mater. Interfaces* **7**, 15042–15051 (2015)
7. Zare, K., Gupta, V.K., Moradi, O., Makhlof, A.S.H., Sillanpää, M., Nadagouda, M.N., Sadegh, H., Shahryari-ghoshekandi, R., Pal, A., Wang, Z., Tyagi, T., Kazemi, M.: A comparative study on the basis of adsorption capacity between CNTs and activated carbon as adsorbents for removal of noxious synthetic dyes: a review. *J. Nanostruct. Chem.* **5**(2), 227–236 (2015)
8. Moradi, O., Fakhri, A., Adami, S., Adami, S.: Isotherm, thermodynamic, kinetics, and adsorption mechanism studies of Ethidium bromide by single-walled carbon nanotube and carboxylate group functionalized single-walled carbon nanotube. *J. Colloid Interface Sci.* **395**, 224–229 (2013)
9. Abd El Fatah, O., Osmann, M.E.: Removal of heavy metal by nickel oxide nano powder. *Int. J. Environ. Res.* **8**(3), 741–750 (2014)
10. Coston, J.A., Fuller, C.C., Davis, J.A.: Pb²⁺ and Zn²⁺ adsorption by a natural aluminum-and iron-bearing surface coating on an aquifer sand. *Geochim. Cosmochim. Acta* **59**, 3535–3547 (1995)
11. Agrawal, A., Sahu, K.K.: Kinetic and isotherm studies of cadmium adsorption on manganese nodule residue. *J. Hazard. Mater.* **137**, 915–924 (2006)
12. Srivastava, N.K., Jha, M.K., Sreekrishnan, T.R.: Removal of Cr(VI) from waste water using NiO nanoparticles. *Int. Sci. Environ. Technol.* **3**(2), 395–402 (2014)
13. Awasthi, S., Awasthi, K., Kumar, R., Srivastava, O.N.: Functionalization effects on the electrical properties of multi-walled carbon nanotube-polyacrylamide composites. *J. Nanosci. Nanotechnol.* **9**, 5455–5460 (2009)
14. Kumar, R., Singh, R.K., Ghosh, A.K., Sen, R., Srivastava, S.K., Tiwari, R.S., Srivastava, O.N.: Synthesis of coal-derived single-walled carbon nanotube from coal by varying the ratio of Zr/Ni as bimetallic catalyst. *J. Nanopart. Res.* **15**, 1406 (2013)
15. Kumar, R., Singh, R.K., Singh, D.P.: Natural and waste hydrocarbon precursors for the synthesis of carbon based nanomaterials: graphene and CNTs. *Renew. Sustain. Energy Rev.* **58**, 976–1006 (2016)
16. Li, Y.H., Di, Z., Ding, J., Wu, D., Luan, Z., Zhu, Y.: Adsorption thermodynamic, kinetic and desorption studies of Pb²⁺ on carbon nanotubes. *Water Res.* **39**, 605–609 (2005)
17. Taleshi, F., Hosseini, A.A.: Synthesis of uniform MgO/CNT nanorods by precipitation method. *J. Nanostruct. Chem.* **3**(1), 1–5 (2012)
18. Jiang, S., Storr Handberg, E., Liu, F., Liao, Y., Wang, H., Li, Z., Song, S.: Effect of doping the nitrogen into carbon nanotubes on the activity of NiO catalysts for the oxidation removal of toluene. *Appl. Catal. B* **160–161**, 716–721 (2014)
19. Song, S., Meng, A., Jiang, S., Cheng, B., Jiang, C.: Construction of Z-scheme Ag₂CO₃/N-doped graphene photocatalysts with enhanced visible-light photocatalytic activity by tuning the nitrogen species. *Appl. Surf. Sci.* **396**, 1368–1374 (2017)
20. Taleshi, F., Porkia, M., Shakeri Chenari, I., Pahlavan, A., Ahmadi Tarsi, M., Zabihi, F., Dehghan-niarostami, N.: Morphology of CuFe₂O₄/CNT composites prepared by precipitation, plastics, rubber and composites. *Macromol. Eng.* **43**, 240–244 (2014)
21. Han, W.Q., Zettl, A.: Coating single-walled carbon nanotubes with tin oxide. *Nano Lett.* **3**, 681–683 (2003)
22. Mallick, P., Chandanarath Biswal, R., Mishra, N.C.: Structural and magnetic properties of Fe doped NiO. *Indian J. Phys.* **83**, 517–523 (2009)
23. Mallick, P., Sahoo, C.S., Mishra, N.C.: Structural and optical characterization of NiO nanoparticles synthesized by sol-gel route. *AIP Conf. Proc.* **1461**, 229–232 (2012)
24. Takami, S., Hayakawa, R., Wakayama, Y., Chikyow, T.: Continuous hydrothermal synthesis of nickel oxide nanoplates and their use as nanoinks for p-type channel material in a bottom-gate field-effect transistor. *Nanotechnology* **21**, 134009 (2010)
25. Yudin, A., Shatrova, N., Khaydarov, B., Kuznetsov, D., Dzidziguri, E., Issi, J.P.: Synthesis of hollow nanostructured nickel oxide microspheres by ultrasonic spray atomization. *J. Aerosol Sci.* **98**, 30–40 (2016)
26. Chakrabarty, S., Chatterjee, K.: Synthesis and characterization of nanodimensional NiO semiconductor. *J. Phys. Sci.* **13**, 245–250 (2008)
27. Lin, P., She, Q., Hong, B., Liu, X., Shi, Y., Shi, Z., Zheng, M., Donga, Q.: The nickel oxide/CNT composites with high capacitance for supercapacitor. *J. Electrochem. Soc.* **157**(7), A818–A823 (2010)
28. Kumar, R., Singh, R.K., Vaz, A.R., Savu, R., Moshkalev, S.A.: Self-assembled and one-step synthesis of interconnected 3D network of Fe₃O₄/reduced graphene oxide nanosheets hybrid for high-performance supercapacitor electrode. *Appl. Mater. Interfaces* **9**, 8880–8890 (2017)
29. Taleshi, F.: A new strategy for increasing the yield of carbon nanotubes by the CVD method. *Fuller. Nanotubes Carbon Nanostruct.* **22**, 921–927 (2014)
30. Gupta, V.K., Agarwal, S., Saleh, T.A.: Synthesis and characterization of alumina-coated carbon nanotubes and their application for lead removal. *J. Hazard. Mater.* **185**, 17–23 (2011)
31. Rao, M.M., Ramesh, A., Rao, G.P.C., Seshiah, K.: Removal of copper and cadmium from the aqueous solutions by activated carbon derived from *Ceiba pentandra* hulls. *J. Hazard. Mater. B* **129**, 123–129 (2006)
32. Tahermansouri, H., Dehghan, Z., Kiani, F.: Phenol adsorption from aqueous solutions by functionalized multiwalled carbon nanotubes with a pyrazoline derivative in the presence of ultrasound. *RSC Adv.* **5**, 44263–44273 (2015)
33. Langmuir, I.: The adsorption of gases on plane surfaces of glass, mica and platinum. *J. Am. Chem. Soc.* **40**, 1361–1403 (1918)
34. Freundlich, H.: Over the adsorption in solution. *J. Phys. Chem.* **57**, 385–470 (1906)
35. Li, Y.H., Wang, S., Wei, J., Zhang, X., Xu, C., Luan, Z., Wei, B.: Lead adsorption on carbon nanotubes. *Chem. Phys. Lett.* **357**, 263–266 (2002)
36. Chen, Y., Haddon, R.C., Fang, S., Rao, A.M., Eklund, P.C., Lee, W.H., Smalley, R.E.: Chemical attachment of organic functional

- groups to single-walled carbon nanotube material. *J. Mater. Res.* **13**, 2423–2431 (1998)
37. Imamoglu, M., Tekir, O.: Removal of copper(II) and lead(II) ions from aqueous solutions by adsorption on activated carbon from a new precursor hazelnut husks. *Desalination* **228**, 108–113 (2008)
38. Xu, D., Tan, X., Chen, C., Wang, X.: Removal of Pb(II) from aqueous solution by oxidized multiwalled carbon nanotubes. *J. Hazard. Mater.* **154**, 407–416 (2008)
39. Perez-Aguilar, N., Muñoz-Sandoval, E., Diaz-Flores, P., Rangel-Mendez, J.: Adsorption of cadmium and lead onto oxidized nitrogendoped multiwall carbon nanotubes in aqueous solution: equilibrium and kinetics. *J. Nanopart. Res.* **12**, 467–480 (2010)
40. Jahangiri, M., Kiani, F., Tahermansouri, H., Rajabalinezhad, A.: The removal of lead ions from aqueous solutions by modified multi-walled carbon nanotubes with 1-isatin-3-thiosemicarbazone. *J. Mol. Liq.* **212**, 219–226 (2015)
41. Zhang, C., Sui, J., Li, J., Tang, Y., Cai, W.: Efficient removal of heavy metal ions by thiol functionalized superparamagnetic carbon nanotubes. *Chem. Eng. J.* **210**, 45–52 (2012)
42. Saleh, T.A.: Nanocomposite of carbon nanotubes/silica nanoparticles and their use for adsorption of Pb(II): from surface properties to sorption mechanism. *Desalin. Water Treat.* **57**, 10730–10744 (2016)
43. Hu, J., Shao, D., Chen, C., Sheng, G., Li, J., Wang, X., Nagatsu, M.: Plasma-induced grafting of cyclodextrin onto multiwall carbon nanotube/iron oxides for adsorbent application. *J. Phys. Chem. B* **114**, 6779–6785 (2010)
44. Hsieh, S.H., Horng, J.J.: Adsorption behavior of heavy metal ions by carbon nanotubes grown on microsized Al_2O_3 particles. *J. Univ. Sci. Technol.* **14**, 77–84 (2007)
45. Yang, S., Hu, J., Chen, C., Shao, D., Wang, X.: Mutual effects of Pb(II) and humic acid adsorption on multiwalled carbon nanotubes/polyacrylamide composites from aqueous solutions. *Environ. Sci. Technol.* **45**, 3621–3627 (2011)
46. Ouki, S.K., Kavannagh, M.: Performance of natural zeolites for the treatment of mixed metal-contaminated effluents. *Waste Manag. Res.* **15**, 383–394 (1997)
47. Benguell, B., Benaissa, H.: Cadmium removal from aqueous solutions by chitin: kinetic and equilibrium studies. *Water Res.* **36**, 2463–2474 (2002)
48. Gu, H., Lou, H., Tian, J., Liu, S., Tang, Y.: Reproducible magnetic carbon nanocomposites derived from polystyrene with superior tetrabromobisphenol A adsorption performance. *J. Mater. Chem. A* **4**, 10174–10185 (2016)
49. Gu, H., Lou, H., Ling, D., Xiang, B., Guo, Z.: Polystyrene controlled growth of zerovalent nanoiron/magnetite on a sponge-like carbon matrix towards effective Cr(VI) removal from polluted water. *RSC Adv.* **6**, 110134–110145 (2016)

